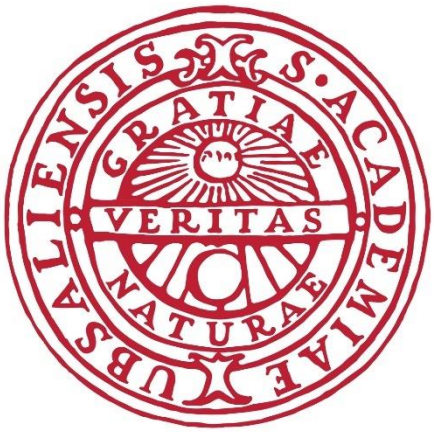

UPPSALA UNIVERSITET

15 Credits Project work in Physics & Astronomy (2018)

Spectral investigation of the globular cluster M30

Kilian Hikaru Scheutwinkel

Supervised by Andreas Korn at the Department of Physics and Astronomy

Abstract

Globular cluster studies suggest that a signature in the spectra of RGB stars in a globular cluster are anti-correlations in Mg-Al and Na-O. In this work, a small sample of 12 RGB stars of the globular cluster M30 is investigated using VLT-UVES high-resolution spectrograph. I use photometric stellar parameters to derive the abundances of Fe, Na, Al and Mg in SIU – a visual spectral analysis tool using 1-dimensional hydrostatic plane parallel MAFAGS atmospheres assuming mixing length convection and treating line formation in LTE. We found signatures of Mg-Al anti-correlation in M30 with the majority of the stars belonging to the intermediate polluted group. Oxygen couldn't be measured but an indirect clue to the Na-O anti-correlation is found due to the direct correlation of Al-Na. These results are consistent with recent studies of other globular clusters.

Introduction

Globular clusters (GCs) are a collection of thousands of stars which form a spherical object due to their strongly gravitational bounding and they are more dense towards the center. GCs are orbiting the galactic center as satellites, hence they belong to a halo of a galaxy or thick disk population (Zinn 1985, Da Costa & Armandroff 1995). In general, the metallicity of a GC is an indication of the age of a GC because heavier elements are synthetized by stellar nucleosynthesis and these elements are recycled by the next population/formation of stars. Therefore, older stars are likely to have a lower metallicity. The exact process of GC formation is still unknown but it is known that most of the stars in a GC are within the same stage in stellar evolution, suggesting a formation history in the same epoch (Chaboyer 2001). However, recent studies discovered that there are multiple populations of stars in galactic GCs which all have different chemical compositions shown by spectroscopy and photometric studies (Gratton, Carretta, Bragaglia 2012). Indications of unexpected abundance patterns of CH and CN in the red giant branch (RGB) of GCs were already found in the seventies (Osborn 1971) leading to the discovery of the CH-CN anti-correlation in main sequence (MS) stars of NGC 6752 (Suntze & Smith 1991), 47 Tuc (Cannon et al.1998), and M 71 (Cohen 1999a). Evidences for a second anti-correlation - the Na-O anti-correlation and the Na-Al correlation - was found almost two decades ago in some giants belonging to GCs (Smith 1987 & Kraft 1994). At this time, it was hard to understand how stars with almost the same age and evolutionary stage showed a significant difference in abundances. One common explanation was deep mixing in RGB stars caused by meridional circulations (Sweigart & Mengel 1979; Charbonnel,1994; Denissenkov & Tout 2000). Until observations of MS stars of a GC (Gratton et al. 2001) unveiled that the Na & Al enhancement with Mg & O depletion is caused by a stellar pollution of a previous population, since MS stars do not have a convective envelope deep enough to allow deep mixing. By now, the Na-O anti-correlation is the best-studied chemical relation discovered by the Lick-Texas group (Kraft 1994, Sneden 2000) and is considered a property of GC stars (Carretta et al. 2010). The typical “shape” of Al-Mg & Na-O anti-correlation and Na-Al correlation can be seen in e.g. Figure 1 of Carretta 2016 (reproduced in appendix).
In this work, I try to observe the Mg-Al anti-correlation and the Na-Al correlation, as a substitute of the Na-O anti-correlation, along the red giant branch in the globular cluster M30. 12 stars are observed with the fiber-fed ESO-VLT UVES spectrograph and I derive the abundances of Fe, Mg, Na, and Al. The observations and the resulting data reduction and processing are described in section 2. The determination of the chemical abundances is presented in section 3, whereas the resulting Mg-Al anti-correlation and the Na-Al correlation is presented in section 4. Finally, I summarize the whole work in section 5.

2. Observations and Data Reduction

The observations were prepared by my supervisor Andreas Korn (PI: Pieter Gruyters) and the observations at the European Southern Observatories (ESO) were done on the Very Large Telescope (VLT) in service mode. The VLT consists of four telescopes with 8.2 m diameter. The telescopes can be operated individually or work together to form the ESO VLT Interferometer. The spectrograph used for this work is the Ultraviolet and Visual Echelle Spectrograph (UVES) on unit telescope 2.

UVES is a high-resolution optical spectrograph attached to one of the four telescopes (UT2). The light passing through UVES will be split into a blue and red part of the optical wavelength range. For this work, 12 stars of M30 with magnitudes in the V band between 12 and 18 were investigated.

2.1. Data reduction

The acquired raw data were uploaded onto the ESO archive and have to be reduced after download. ESO offers an automatic data reduction pipeline for the UVES spectrograph – the ESO Reflex pipeline (Freudling et al., 2013). The Reflex pipeline does all the basic steps (e.g. bias subtraction, flat-fielding and wavelength calibration) to output the final 1-dimensional spectra of each star in the red and blue part of the visible wavelength area. A graphical overview of the Reflex pipeline environment is shown in Figure 1.

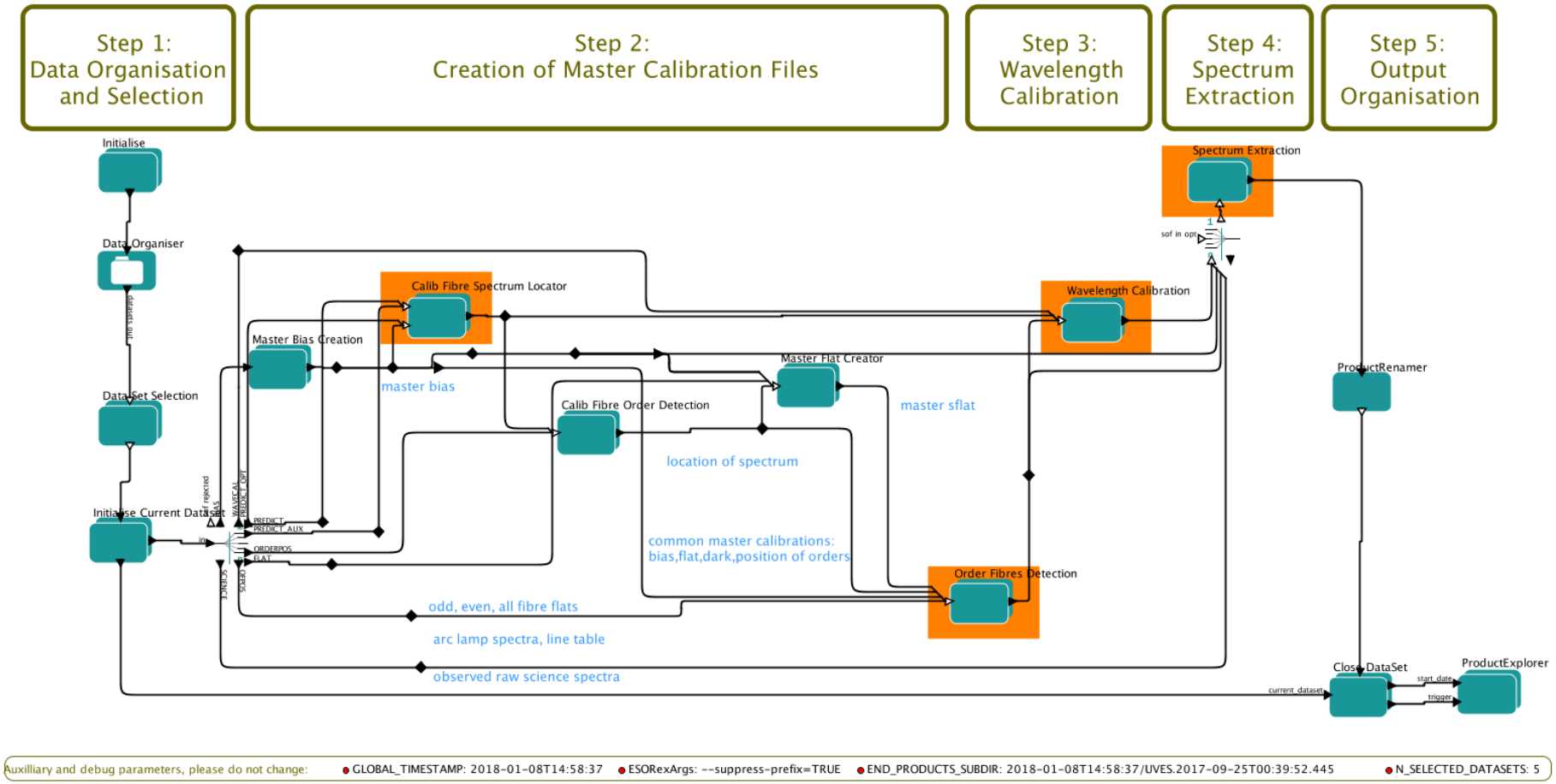

Figure 1: The ESO Reflex pipeline graphical overview. This pipeline does all the necessary data-reduction steps e.g. bias subtraction, flat-fielding etc (Freudling et al. 2013).

2.2. Data processing

In total 33 Observing Blocks (OBs) of 1 hour each were executed and each star has been observed around 15-20 times except one sub-giant - namely M30-1966, which has been observed 33 times. For each observation, a plate consisting of 8 fibers (1 sky fiber, 1 M30-1965 fiber, and 6 M30 stars) has been used. There were in total 2 plates with the same amount of fibers but one plate has a broken fiber in which no light will be detected. On this broken fiber, a star called M30-210 was put, which is already observed on the other plate. The deciding factor to sort the stars into one setup was the photometric V magnitude of each star, as too large a magnitude difference between stars could lead to cross talk on the CCD. Therefore, one setup consists of bright targets (12 – 14 mag) and the other setup consists of faint targets (14 – 18 mag).

Now, each object has a blue and red output and each OB has a "fiber-to-object" identification file after the Reflex Pipeline data reduction. A problem of identification uniqueness can occur when a broken fiber exists. The identification file will show an empty slot at the position n of the broken fiber, whereas the total numbering N of the output files is shifted to N-1. This can lead to the following problem: The empty slot has still the same file numbering as a plate without the broken fiber and all following stars keep their usual file numbering. Or, the empty slot leads to a numbering shift e.g. file 7 belonging to star 6 is now belonging to star 5. The latter was the case as spectra inspection showed. After sorting the correct files for each star, the next step is to sky-subtract the spectra, then radial-velocity correct each one. Finally, the spectra of each star can be co-added to improve the Signal-to-Noise ratio (S/N).

2.2.1 Sky subtraction

Sky subtraction of each spectrum is necessary to avoid contamination of spectral lines by sky lines and solar light (scattered moonlight). The contamination originates from the reflected sunlight onto the moon, the telluric lines from the Earth's atmosphere. Each contribution can have a serious impact on abundance determination. The reflected sunlight contains the sun spectra which is 2.3 dex more metal rich (~200 times) than our targets in M30. Therefore, targets which have stellar parameters close to our sun have the same metal lines. Hence, an object which is very faint with very narrow metal lines compared to the broad metal lines of the sun can be contaminated tremendously by falsely broadening the wings of a line. The same impact is seen at the strong emission lines of telluric lines.

To minimize this contamination, for each observation one sky-fiber is pointed to a sky location close to M30 in which no object is located. The obtained sky-spectra can then be subtracted from the star spectra.

To identify the sky fiber is simple: First, the "fiber-to-object" identification file will tell you which fiber is supposed to be the sky fiber. Second, by investigating the spectra a sky spectrum has almost no continuum flux compared to a star spectrum. Third, the sky-spectra has a lot of strong emission lines & telluric lines compared to the continuum flux. For the bright setup, the sky is located on fiber 6 and for the faint setup the sky is located on fiber 2.

2.2.2 Radial-velocity correction

Radial-velocity correction of each observation for each star is needed because a star is not fixed on the sky even though it appears to be for the human eye. There are several movements contributing to the radial velocity of a target:

First, the night sky is rotating due to the Earths rotation around its own axis. This rotation is mostly automatically corrected by moving the telescope along with the target. Second, the revolution of the Earth around the Sun changes the relative movement to the object. Third, the globular cluster has its own relative motion to the telescope. And finally, the stars within a globular cluster also have relative movement to the GCs movement. These movements lead to Doppler-shifted spectra for each individual star and OB. Hence, before co-addition, the spectra have to be radial-velocity corrected to the heliocentric system. The principle is simple: One uses the sun spectrum in the heliocentric system, compare this spectrum with the individual observations and then shift the observations so the spectral lines will match. Since the targets are 200 times more metal poor than the sun, the reference lines for 1-dimensional shifting should be strong prominent lines (e.g. magnesium triplet lines, Balmer Hα, Hβ or Fe II lines) which are visible in the metal-poor stars.

In practice, I have used a script routine using IRAF tasks to automatically radial-velocity correct each spectrum. The main tasks can be described with the following steps:

1. Extract observation and target information from the fits Header
2. Import the high-S/N Kitt-Peak Solar Atlas (Kurucz et al. 1984) as reference spectrum
3. Using the fxcor IRAF task for wavelength shifting

Since the targets are very faint and metal-poor ([Fe/H] = -2.3[a]) I have used a wavelength window of 100 Å around Balmer Hβ or Hα. For the brighter targets, the radial-velocity correction was not a problem, whereas for the fainter targets the window had to be narrowed to 50 Å. In theory, the Balmer lines are enough to apply the wavelength shifting but since the Balmer lines are very broad, the identification of the line center is more vulnerable to errors than when using narrow metallic lines. This has led me to discard three spectra on average for the very faint targets. In addition, for the subgiant M30-1966, the S/N ratio was so low, that a correct identification with the fxcor task was not possible for the blue part. I tried to do the radial velocity correction manually by using the results of the radial velocity correction of the red spectra. But in the following quality check, there were almost no metallic lines visible leading to omitting the subgiant altogether.

[a] Metallicity of iron is defined as:

$$\left[\frac{Fe}{H}\right] = log_{10}\left(\frac{N_{Fe,star}}{N_{H,star}}\right) - log_{10}\left(\frac{N_{Fe,sun}}{N_{H,sun}}\right)$$

hence [Fe/H] = 0 is solar metallicity.

Table 1: Radial Velocity Statistics for each M30 star. The mean radial velocity for the cluster is -183.4 km/s (Harris, 1996)

Target Name	$\overline{RV}$ blue [km/s]	σ_{RV} blue [km/s]	$\overline{RV}$ red [km/s]	σ_{RV} red [km/s]
M30_1498	-184.642	0.213	-184.472	0.467
M30_3630	-185.744	0.637	-185.444	0.665
M30_6475	-186.236	0.254	-185.956	0.232
M30_1884	-194.824	0.4852	-194.346	0.5774
M30_201180	-187.936	0.316	-187.558	0.335
faint M30_751	-180.436	0.765	-180.512	0.3973
M30_210	-186.515	0.426	-186.44	0.362
M30_6044	-184.474	0.428	-184.414	0.425
M30_1945	-189.81	0.431	-189.868	0.388
M30_6064	-191.218	0.5764	-191.138	0.3729
M30_4985	-184.32	0.497	-184.193	0.5274
M30_1966	?	?	?	?

Furthermore, heliocentric corrected radial velocities unveil how a star moves relative to the telescope. Since our work is focused on isolated stars, hence no binary systems, the individual radial velocities per observation night should not be periodic throughout the observation period (Figure 2), which is the case.

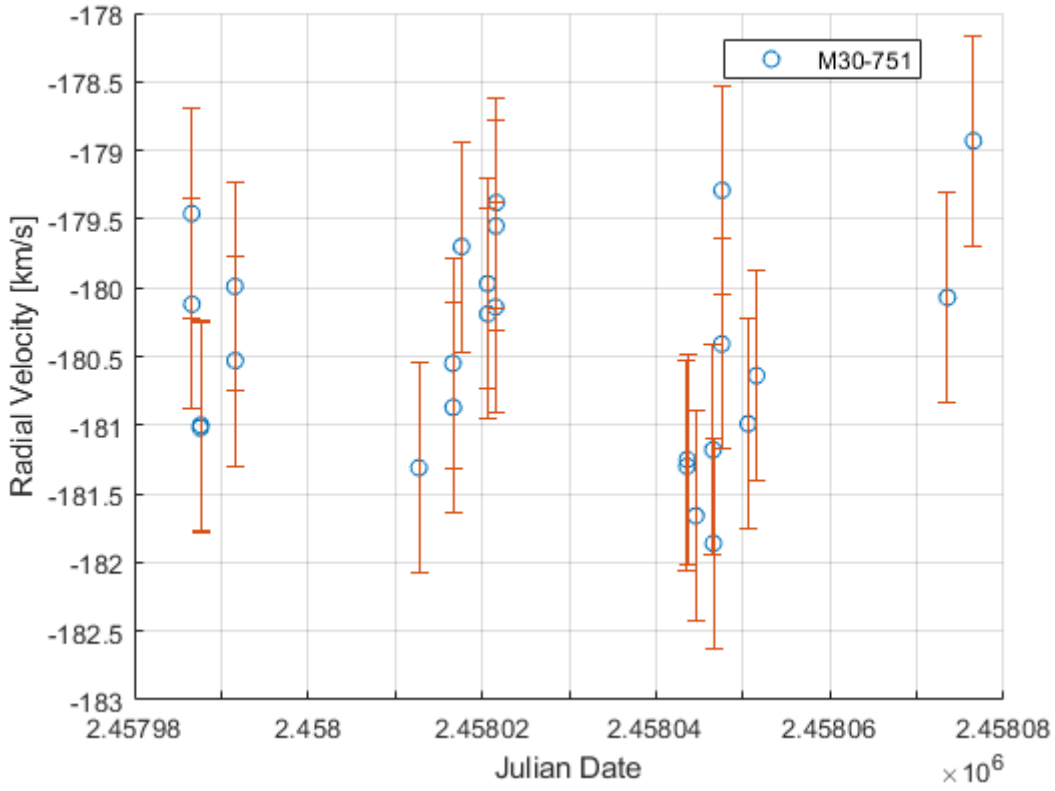

Figure 2: The radial velocities for the RGB star M30-751 shows no significant variability throughout the observation period, hence it is unlikely to be a binary system detectable at this level of data quality.

2.2.3. Co-addition and inspection

After all spectra are now radial velocity corrected, the co-addition of each individual star can be applied. The purpose is to significantly improve the S/N for each star. Also, cosmic rays which hit the CCD and leave an artifact in a spectrum can be removed efficiently because it is very unlikely that a particle hits the same CCD pixel twice. The co-addition is done by the IRAF task scombine.

After the co-addition an inspection of the output spectra by measuring the S/N ratios has been done. IRAF provides a very convenient way to measure the S/N ratio in a line-free wavelength region. In the splot environment, one uses the “m” key button around 6376 Å to automatically compute the mean, root mean square and the S/N ratio. Overall, the S/N ratio for all stars except the subgiant M30-1966 meets the expectations (Table 2 in appendix & Figure 3)

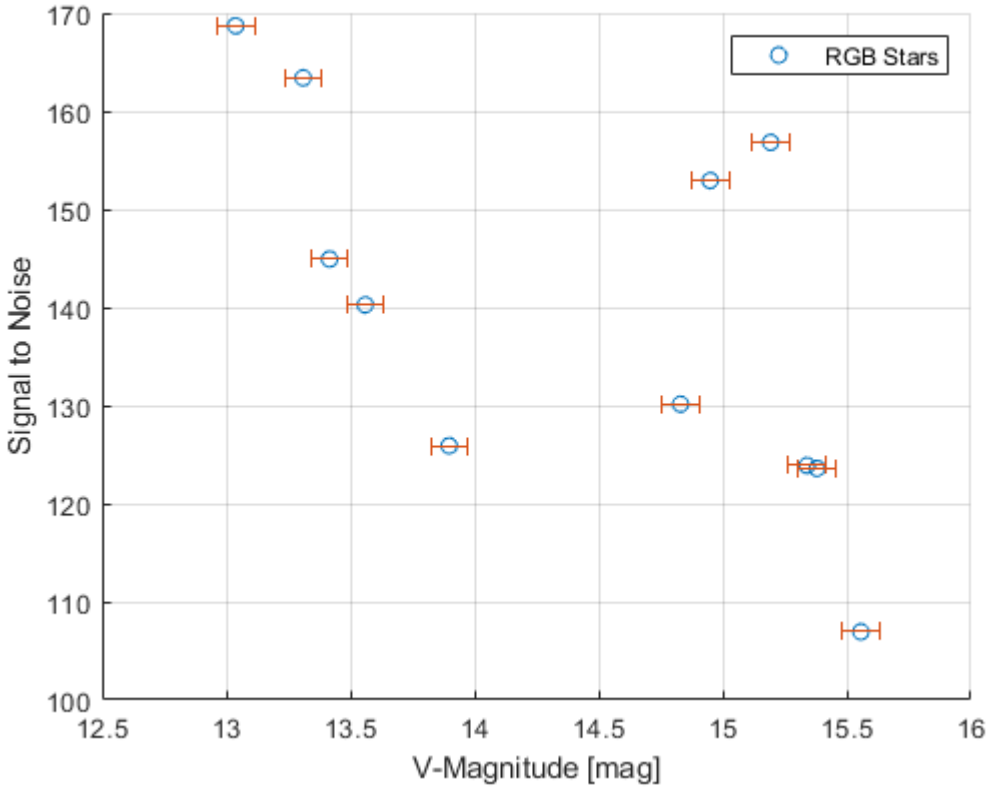

Figure 3: The S/N ratio is overall decreasing the fainter the stars are

3. Chemical Abundances

To determine chemical abundances one needs the stellar parameters. There are three main stellar parameters which have to be known to accurately calculate the abundances: the effective temperature, the surface gravity of the star and the metallicity of the star. In this work, I adopt the photometric values derived by Gruyters et al. (2016) using the VI broadband photometry from Peter Stetson (Stetson, 2000 & 2005). The uncertainty is 50 K for T_{eff} which leads to an error of 0.03 dex in log *g* and 0.075 mag in V magnitude (Gruyters et al. 2015). As a starting point, I assume a metallicity of [Fe/H] = -2.3 dex – the metallicity of the globular cluster M30 - for the abundance analysis code. Abundances are derived using the Spectral Investigation Unit (SIU) (Reetz 1991). SIU is a visual spectral abundance analysis code written in IDL to compare the observed spectrum with a synthetic theoretical spectrum. The underlying model in SIU is a grid of hydrostatic 1-dimensional stellar-atmosphere models with plane parallel MAFAGS atmospheres and line formation treated in local thermodynamical equilibrium (LTE) (Fuhrmann et al. 1997, Grupp 2004). Although the model is assumed to be hydrostatic, energy transport by convection is included following a mixing length treatment. In this work, the chemical abundances of iron, magnesium, sodium and aluminium are determined by a line-to-line analysis.

3.1. Iron abundances

In the UVES setting 11 non-blended iron lines (Table 3, appendix) have been visually fitted with SIU (Figure 4) using the most recent log *gf* values (Table 3) - atomic data in which *g* represents the statistical weight of the lower atomic level involved in the transition and *f* the oscillator strength. The line strength varies from really weak lines with an equivalent width (EW) of 10 mÅ to strong lines with an EW of 120 mÅ. Stronger lines will not be considered since they are highly sensitive to the microturbulence parameter ξ and non-LTE effects. The microturbulence parameter is an additional input parameter which represents convection on length scales smaller than the mean-free path of the photons in the line-formation zone. Hydrodynamical models of stellar surface convection have in recent years done away with the micro-/macroturbulence formalism. The microturbulence parameter is needed to ensure constant abundances throughout all line strengths. Because the weakest lines are insensitive to the microturbulence parameter, the abundances of iron are mainly dictated by their EW, whereas the abundances of the strongest lines need to be adjusted to the abundances of the weakest lines. The sensitivity of the chemical abundances to the microtubulence parameter is investigated by changing the initial guess by $\pm$0.1 km/s. Once this value is found – a typical value is about ξ = 1.7 km/s for a RGB star (Figure 5) – each line can be examined to calculate an average of all lines and its standard deviation to determine the stars [Fe/H] value.

However, one should be very careful about the abundance determination of the weakest lines, because a wrong continuum placement can have a huge impact on the EW / iron content. Also, the macroturbulence parameter (Gaussian broadening) should not vary for each line for different stars – typical values are about 4-6 km/s for medium to strong lines. Ideally, the iron content of each star is in agreement with the iron content of the globular cluster M30 and also the individual stars in the RGB should not vary much relative to each other (Figure 6).

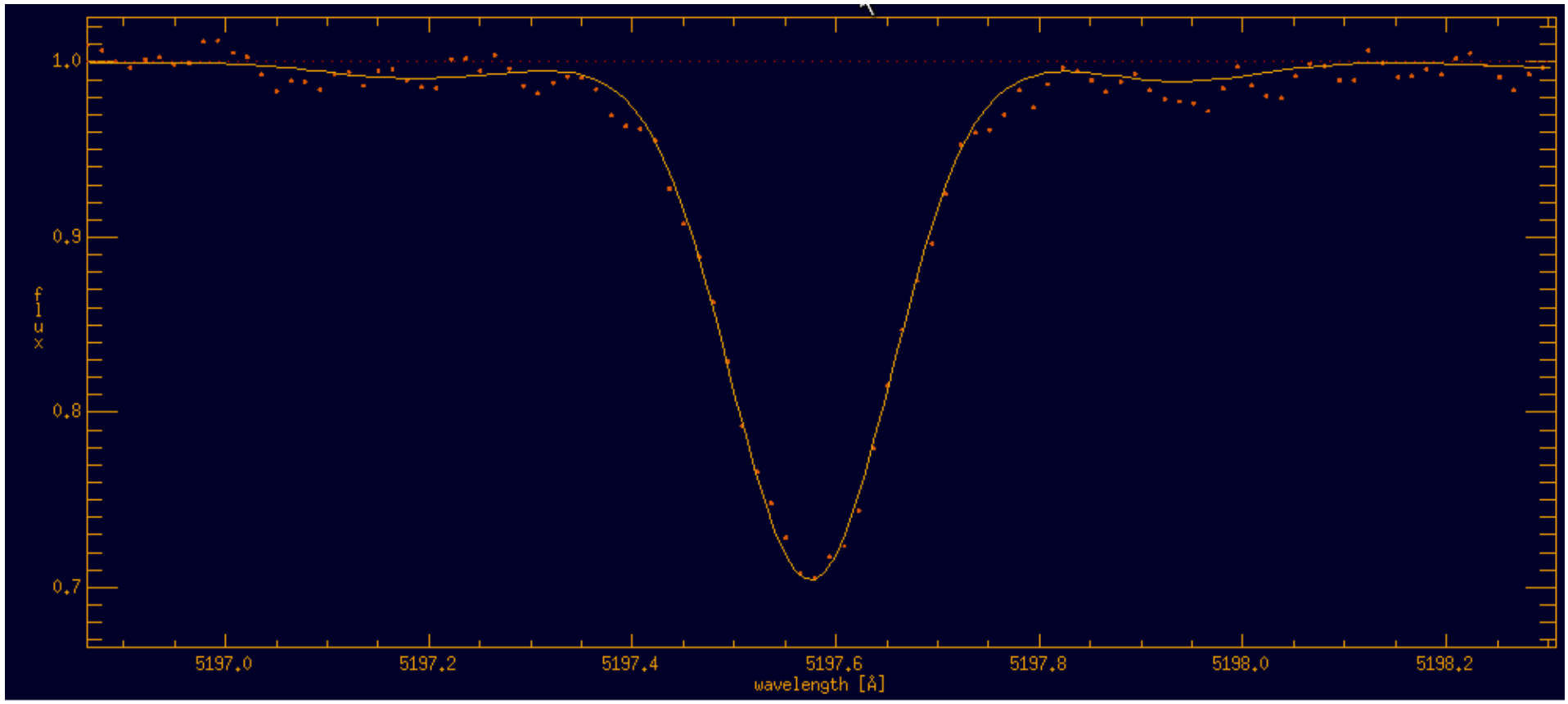

Figure 4: Synthetic fit (yellow solid line) of the observed spectrum (orange pixels) of M30 3630 showing the 5197.6 Å absorption Fe II line

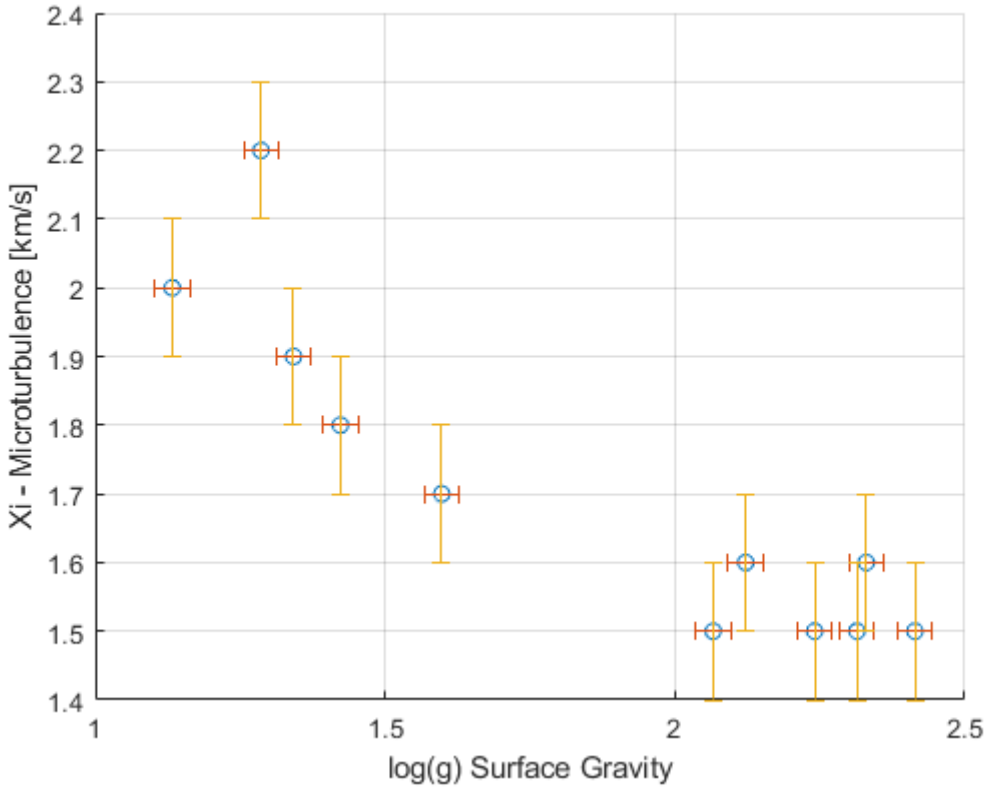

Figure 5: The microturbulence parameter ξ is increasing with decreasing surface gravities of RGBs.

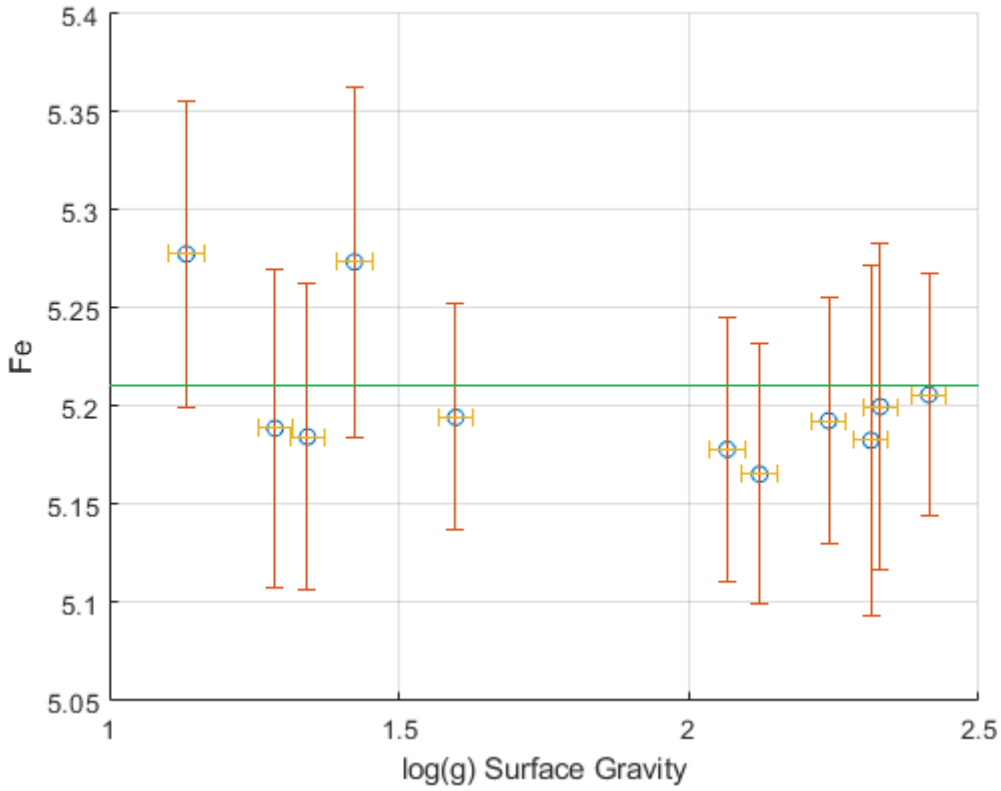

Figure 6: log *g* and the abundances Fe for each star. The iron content of all stars is in agreement within their error bars (1-σ) with the M30 iron content $\log_{\varepsilon}$ Fe = 5.21 (green line)

3.2. Aluminum, sodium and magnesium abundances

After the metallicity of the star and its microturbulence parameter is determined the abundances for aluminum, sodium, and magnesium can be studied. In the UVES setting two weak Na lines (EW ~15 mÅ), two Mg lines (EW ~20 mÅ and ~ 90 mÅ) and one weak Al (EW ~ 10 mÅ) line can be found (Table 4). In some cases the weakest lines are not visible due to the noise level in the continuum, so a 2-sigma synthetic line (Figure 7), in which $1\sigma = (S/N)^{-1}$, is fit into the noise and assumed to be the upper limit. Also, in this UVES setting there should be in total four Na lines visible, but due to their weakness only two can be observed and measured in every star. Oxygen lines were not visible in the UVES setup.

Fe, Na, and Mg have enough (>1) detectable absorption lines to determine its standard deviation of abundances - typical values are in the range of 0.1 dex. However, there are spectra with lower S/N ratios in which there is only one absorption line visible. In this case, especially with Al which has only one visible line in the UVES setup, I made a sensitivity study with SIU. I used the uncertainty of the photometric parameters T_{eff} and log g of Gruyters et al. (2015) and calculated the maximum abundance deviations I can get with the underlying model of SIU. The outcome was in the order of 0.05 dex, which is not close to the typical uncertainty of 0.1 dex. Therefore, the error of stellar parameters alone is not representative for the absolute error in abundances. So I set the uncertainty for spectra with only one detectable absorption line to 0.1 dex.

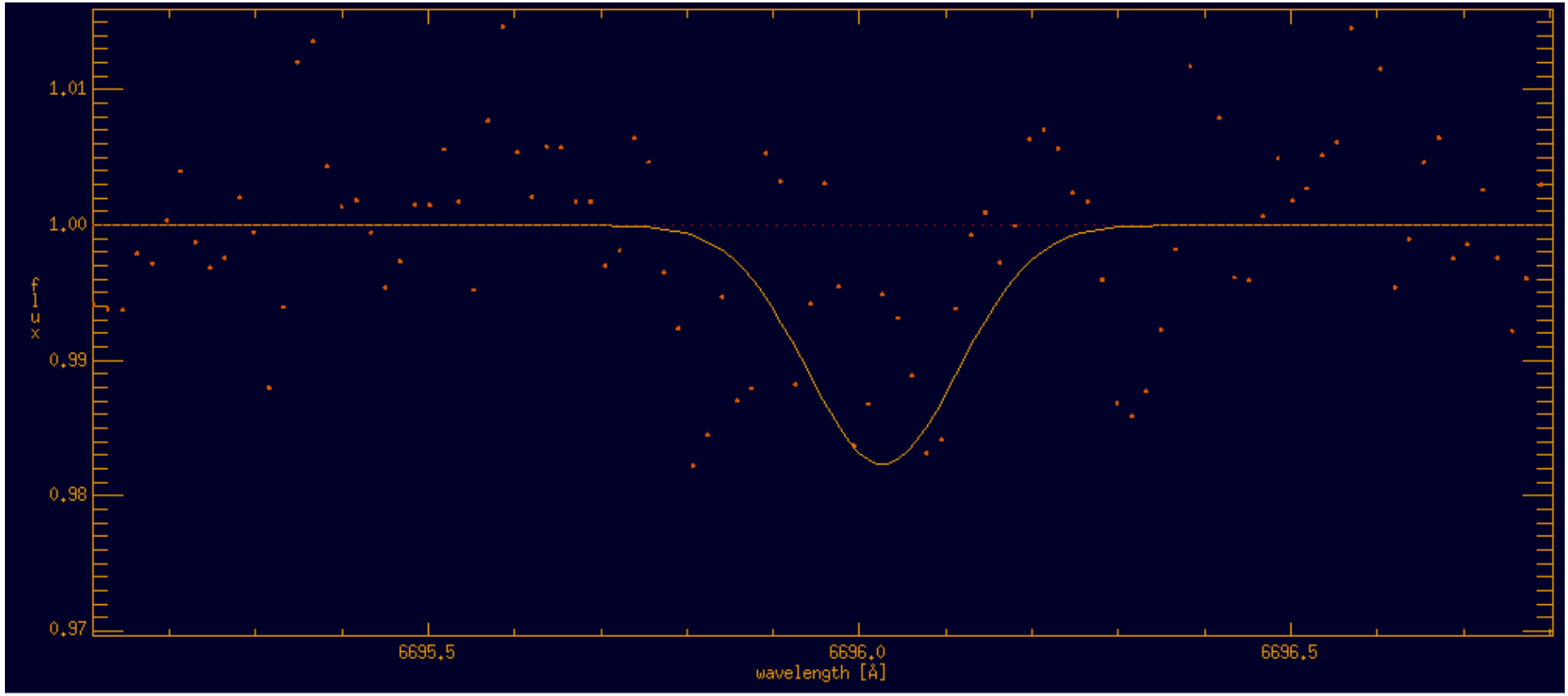

Figure 7: The 2-σ upper limit fit (yellow solid line) in the observed spectrum (orange pixels) of M30 6064 at 6696.0 Å of Al.

4.Results & Discussion

The outcome of the abundance study of Mg, Al and Na are shown in Figure 8 & 9. One can see a trend to an anti-correlation in Mg & Al. Two stars (M30 201180 & M30 1884) belong to the primordial population – a population in which Al is not enriched at the cost of Mg. The rest belong to the intermediate population, in which stellar pollution enriches Al at the cost of Mg. The overall plot shows a hint of a curved distribution, which is the typical signature of the Mg-Al anti-correlation (e.g. Figure 1, Carretta 2016). However, 4 out of 11 stars (Table 2) are only 2-sigma upper limits of Al, and can significantly bias the overall „banana-shape“, especially the star with the lowest Mg content. Thus, one needs more data to improve the statistical foundation of the results. The Al-Na plot shows a significant linear correlation because these two elements are the anti-correlated partner elements of the alpha-enhanced elements Mg and O. The error bars of Al are set to 0.1 dex, a typical 1-sigma standard deviation. Overall, both plots are consistent with other studies (Gratton, Carretta, Bragaglia 2012, Gratton et al. 2015, Pancino et al. 2017) of GCs and can be improved further by gathering more data of RGB stars in M30.

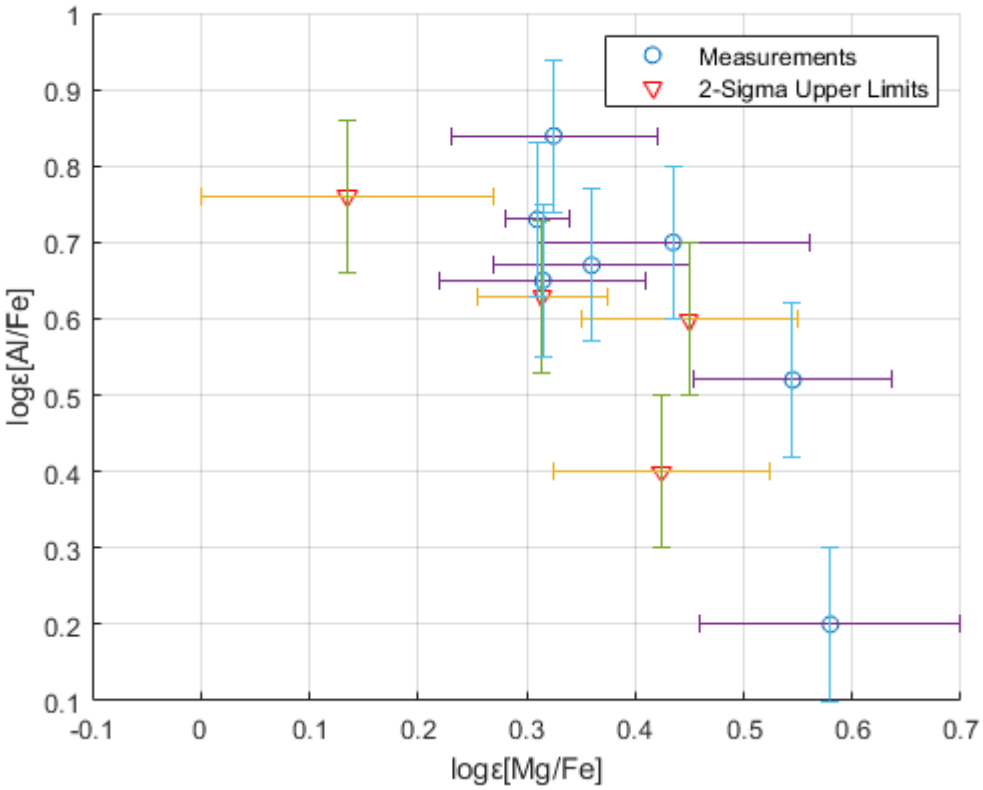

Figure 8: Mg-Al plot shows a slightly curved distribution, which is expected for an Mg-Al anti-correlation

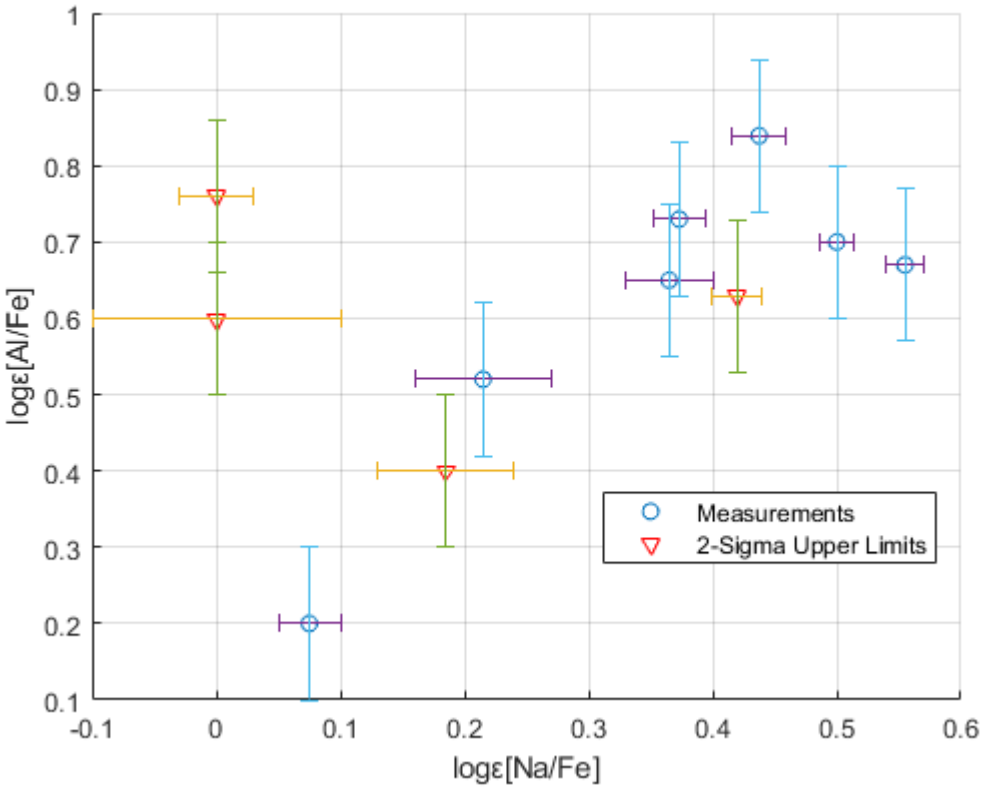

Figure 9: Na-Al plot shows a significant correlation, which is expected (e.g. Figure 1 of Carretta 2016, reproduced in appendix) if Mg-Al and Na-O is correlating

5. Summary

12 stars of the globular cluster M30 have been observed by the ESO-VLT UVES spectrograph in the fiber-fed mode. After the data reduction with the ESO Reflex pipeline and the data processing with IRAF the lithium rich subgiant M30-1966 has to be excluded from further analysis. The reason is the low S/N ratio of the individual spectra because of its low V magnitude (~17.8 mag).

The abundance analysis is done in SIU, a visual spectral analysis tool, which uses 1-dimensional plane parallel hydrostatic MAFAGS atmospheres (Grupp 2004) assuming mixing length convection and treating line formation at LTE conditions. There are three main stellar inputs in SIU: The surface temperature, the surface gravity and the metallicity of each star. For further analysis, I use photometrically derived parameters by Gruyters et al. (2016) using VI broadband photometry (Stetson 2000 & 2005).

First, the iron abundance of each star is determined. I use eleven Fe II lines with varying line strength (EW: 10 – 120 mÅ) to derive the microturbulence parameter for each star. The microturbulence parameter is an additional input parameter in SIU. This parameter ensures constant abundances throughout all line strengths and represents convection on scales smaller than the mean-free path of photons. The resulting metallicities for each star are in agreement with the metallicity of the globular cluster M30.

Second, the abundances of magnesium, sodium, and aluminum are derived with the same method as iron, assuming the same microturbulence parameter for each star. For 4 out of 11 stars, the S/N ratio is not high enough to detect the aluminum line at 6696 Å so I derived a 2-sigma upper limit abundance in which $1\sigma = (S/N)^{-1}$. The macroturbulence parameter (Gaussian broadening) is empirically set to values (~5 km/s) compatible with the line fits.

Finally, I plot the Mg-Al anti-correlation and the Na-Al correlation, since we did not observe oxygen with UVES. The Mg-Al anti-correlation is consistent with other spectral analysis studies of globular clusters. Also, the Na-Al correlation shows an indirect clue to the Na-O anti-correlation as a result of being the partner elements of the alpha enhanced elements. The majority of the stars are in the intermediate polluted population and two in the primordial population, as expected. Since 4 out of 11 stars only provide constraints based on 2-sigma upper limits, more data is needed to improve the statistics and to accurately show that M30 also has these abundance correlations.

Reference

Cannon, R.D., Croke, B.F.W., Bell, R.A., Hesser, J.E., & Stathakis, R.A .1998, MNRAS, 298, 601

Carretta, E., Bragaglia, A., Gratton, R.G., Recio-Blanco, A., Lucatello, S., D'Orazi, V., Cassisi, S. 2010, A&A, 516, 55

Carretta, E.,2016, eprint arXiv:1611.04728, Invited review talk given on August, 10 2016 at the Conference "Star Clusters: From Infancy to Teenagehood", Heidelberg; 23 pages, 19 figures

Chaboyer, B., Astrophysical Ages and Times Scales, ASP Conference Series Vol. 245. p.162

Charbonnel, C., 1994, A&A, 282, 811

Cohen, J.G .1999a, AJ, 117, 2428

Da Costa, G. S. & Armandroff, T. E. 1995, ApJ, 109, 2533

Denissenkov, P.A., & Tout,C.A., 2000, MNRAS,316,395

Freudling, W. et al., 2013, Astron.Astrophys., 559, A96

Fuhrmann, K., Pfeiffer, M., Frank, C., Reetz, J., & Gehren, T. 1997, A&A, 323, 909

Gratton, R.G., Bonifacio, P., Bragaglia, A., et al. 2001, A&A, 369, 87

Gratton, R.G., Carretta, E., Bragaglia, A. 2012, A&ARv, 20, 50

Gratton, R.G. et al. 2015, Highlights of Astronomy, 16, pp. 230-231

Grupp, F. 2004, A&A, 420, 289

Gruyters, P. et al., 2013, A&A, 555, A31

Gruyters, P. et al.,2015, DiVA, id: diva2:739571

Gruyters, P. et al., 2016, A&A, 589, A61, 12 pp.

Harris, William E. 1996, Astronomical Journal, 112, p.1487

Kraft, R.P. 1994, PASP, 106, 553

Kurucz, R. L. et al. 1984, Solar flux atlas from 296 to 1300 nm

Meléndez, J. & Barbuy, 2009, B., Astronomy & Astrophysics, 497, pp.611-617

Osborn,W .1971 Observatory, 91, 223

Pancino, E. et al. Astronomy & Astrophysics, 601, A112, 10 pp.

Reetz, J. K. 1991, Diploma Thesis, University of Munich (LMU)

Smith, G.H. 1987, PASP, 99, 67

Sneden, C. 2000, in "The Galactic Halo : From Globular Cluster to Field Stars", Proceedings of the 35th Liege International Astrophysics Colloquium,1999. Eds. A. Noels, P. Magain, D. Caro, E. Jehin, G. Parmentier, and A. A. Thoul. Liege, Belgium, 2000., p.159

Stetson, P. B. 2000, PASP, 112, 925

Stetson, P. B. 2005, PASP, 117, 563

Suntze, N.B., & Smith,V .1991, ApJ, 381, 160

Sweigart,A .V .,& Mengel, J.G .1979, ApJ, 229, 624

Zinn, R. 1985, ApJ, 293, 424

Appendix

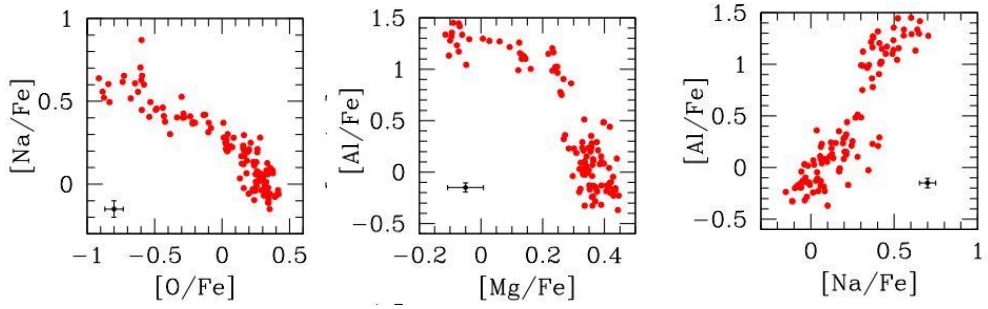

Figure 10: Reproduced excerpts of Figure 1 of Carretta 2016, showing the Na-O & Mg-Al anti-correlations and the Al-Na correlation.

Table 2: Stellar parameters for each M30 star, red values indicates 2-σ upper limits and green stars are primordial.

M30 star	S/N ratio	V [mag]	T_{eff} [K]	log *g*	$\log_\varepsilon$ (Fe)	$\log_\varepsilon$ (Mg)	$\log_\varepsilon$ (Na)	$\log_\varepsilon$ (Al)
1498	125	13.89	4750	1.59	5.19	5.55	5.74	5.86
1884	144	13.41	4642	1.34	5.18	5.76	5.25	5.38
1945	152	14.95	4956	2.12	5.16	5.59	5.35	5.56
1966	22	17.73	5491	3.45	?	?	?	?
210	130	14.83	4934	2.06	5.17	5.49	5.54	5.82
3630	168	13.03	4552	1.13	5.27	5.60	5.71	6.11
4985	156	15.19	5000	2.24	5.19	5.62	5.69	5.89
6044	123	15.38	5034	2.33	5.19	5.64	5.2	5.79
6064	123	15.34	5028	2.31	5.18	5.49	5.60	5.81
6475	163	13.31	4618	1.28	5.18	5.49	5.56	5.91
751	106	15.55	5064	2.41	5.20	5.34	5.20	5.96
201180	140	13.56	4677	1.42	5.27	5.81	5.48	5.793

Table 3: The absorption lines of Fe II which have been used to derive the iron abundance. The EW are observed values obtained by M30-3630 to indicate the line strength.

Element	Wavelength [Å]	EW [mÅ]	log *gf*
Fe	5018.4	141	-1.100[a]
	5197.6	59	-2.220[a]
	5264.8	17	-3.250[b]
	5276.0	81	-2.010[a]
	5284.1	31	-3.200[b]
	5316.6	112	-1.870[a]
	5325.6	14	-3.324[b]
	5362.9	47	-2.570[a]
	5425.3	12	-3.390[b]
	5534.8	31	-2.750[a]
	6456.4	26	-2.050[a]

a: Meléndez & Barbuy (2009), b: Gruyters et al. (2013)

Table 4: The absorption lines of Mg, Na, and Al which has been used to derive the abundances. The EW are observed values obtained by M30-3630 to indicate the line strength.

Element	Wavelength [Å]	EW [mÅ]	log *gf*
Mg	5528.4	106	-0.498[a]
	5711.1	22	-1.724[a]
Na	5682.6	19	-0.706[a]
	5688.2	31	-0.452[a]
	6154.2	3	-1.547[a]
	6160.7	6	-1.260[a]
Al	6696.0	11	-1.347[a]

a: Gruyters et al. (2013)